Determination of three-dimensional imaging properties of a light microscope system

Partial confocal behavior in epifluorescence microscopy

Yasushi Hiraoka, John W. Sedat, and David A. Agard
Department of Biochemistry and Biophysics and The Howard Hughes Medical Institute, University of California at San Francisco, San Francisco, California 94143-0448

ABSTRACT We have determined the three-dimensional image-forming properties of an epifluorescence microscope for use in obtaining very high resolution three-dimensional images of biological structures by image processing methods. Three-dimensional microscopic data is collected as a series of two-dimensional images recorded at different focal planes. Each of these images contains not only in-focus information from the region around the focal plane, but also out-of-focus contributions from the remainder of the specimen. Once the imaging properties of the microscope system are characterized, powerful image processing methods can be utilized to remove the out-of-focus information and to correct for image distortions. Although theoretical calculations for the behavior of an aberration-free microscope system are available, the properties of real lenses under the conditions used for biological observation are often far from an ideal. For this reason, we have directly determined the image-forming properties of an epifluorescence microscope under conditions relevant to biological observations. Through-focus series of a point object (fluorescently-coated microspheres) were recorded on a charge-coupled device image detector. From these images, the three-dimensional point spread function and its Fourier transform, the optical transfer function, were derived. There were significant differences between the experimental results and the theoretical models which have important implications for image processing. The discrepancies can be explained by imperfections of the microscope system, nonideal observation conditions, and partial confocal effects found to occur with epifluorescence illumination. Understanding the optical behavior of the microscope system has indicated how to optimize specimen preparation, data collection, and processing protocols to obtain significantly improved images.

INTRODUCTION

Light microscopy is unique in its ability to allow biological specimens to be examined as living samples or under conditions that closely approximate the living state. The recent advent of a wide variety of highly selective fluorescent probes (DNA-specific dyes, monoclonal antibodies, calcium- and pH-sensitive fluorescent dyes, etc.; reviewed in Waggoner et al., 1989) adds to the fundamental power of light microscopy the ability to examine the spatial distribution of specific cellular components. With increasing frequency, current questions in cell biology focus on elucidating the spatial relationships of cellular components in three dimensions.

Unfortunately, light microscopes are far from ideal for imaging three-dimensional specimens at high resolution. Three-dimensional data can be collected as a series of images obtained by sequentially incrementing the position of the focal plane. Due to the large depth of field in light microscopes (Sheppard, 1987), however, each of these images contain in-focus information from a region immediately surrounding the focal plane together with out-of-focus contributions from the remainder of the specimen. A fundamental requisite, then, for high-resolution three-dimensional imaging is the ability to remove the out-of-focus information contaminating the observed image. Furthermore, because many biological questions demand optical resolutions approaching or even beyond the deffraction limit, image processing is necessary to extract the maximal amount of information available from the specimen. Such processing methods can be applied to images derived from confocal, as well as nonconfocal, optical sectioning microscopy.

The removal of the out-of-focus information that contaminates each image requires accurate knowledge of the three-dimensional image-forming properties of the microscope. The optical properties of a microscope system are dominated by the behavior of the objective lens, which is the principle image-forming component. Although the high-quality, multielement objective lenses found in modern microscopes have been designed to minimize image distortion in the in-focus plane, residual chromatic, and spherical aberrations, and the finite numerical aperture (NA) all lead to errors when recording images from two-dimensional, and especially from three-dimensional, specimens (see chapter 5 in Inoué, 1986).

The manner in which the optical system of a microscope distorts and degrades the image of an object is best understood in terms of the microscope's point-spread function (PSF) or its Fourier transform, the optical

transfer function (OTF). Both of these functions seek to describe how the image of an ideal point object (a delta function) is spread out in three dimensions by passage through the microscope. Image processing to recover an undegraded image requires accurate knowledge of the OTF. The three-dimensional OTF for a light microscope has been theoretically treated for the case of a diffraction-limited, aberration-free microscope system (Hopkins, 1955; Stokseth, 1969) and useful approximations have been developed for the purposes of numerical evaluation (Stokseth, 1969; Castleman, 1979). Unfortunately, real optical systems are prey to a variety of aberrations and so do not obey these simplified models. This is especially apparent when using high-NA immersion lenses where the assumption of paraxial behavior breaks down. We report here on the use of a cooled, charge-coupled device (CCD) imager to provide sufficient data quality for the direct experimental determination of the complete three-dimensional OTF for an epifluorescence microscope. This analysis revealed several significant differences from the theoretical models, including a partial confocal effect which has important implications for three-dimensional resolution and image processing.

Image formation in three dimensions

The behavior of an imaging system is best described in terms of how an idealized point object would spread out and take on a characteristic shape called the point spread function (PSF). As discussed previously (Castleman, 1979; Agard, 1984; Agard et al., 1989), once the microscope's PSF is known, the way in which an arbitrary image is distorted can be predicted for a linear shift-invariant system by convolving the "true" image with the PSF:

$$i(x, y, z) = \int_{x'} \int_{y'} \int_{z'} \cdot o(x', y', z') \cdot s(x - x', y - y', z - z')\, dx'dy'dz', \quad (1)$$

where i is the observed image, o the object or "true" image, s is the PSF or smearing function, and the z index refers to the focus direction. For a general discussion of convolutions see the relevant sections in Bracewell (1965) or Castleman (1979). It is often convenient to recast Eq. 1 in terms of its Fourier transform:

$$I(u, v, w) = O(u, v, w) \cdot S(u, v, w), \quad (2)$$

where capital letters refer to the Fourier transforms of the corresponding lower-case quantities, (u, v, w) are the Fourier space analogues of (x, y, z), and the convolution is now simplified to a multiplication. The Fourier transform of the PSF (S) is called the optical transfer function (OTF). Hopkins (1955), Stokseth (1969), and Castleman (1979) have all described formulae for approximating the two-dimensional OTF of an objective lens as a function of defocus z, $S_z(u, v)$. The complete three-dimensional OTF, $S(u, v, w)$, can be calculated from a set of two-dimensional OTFs by Fourier transformation:

$$S(u, v, w) = \int_z S_z(u, v) e^{2\pi i z w}\, dz. \quad (3)$$

This Fourier transform can be performed either analytically (Erhardt et al., 1985) or numerically (Agard, 1984). From the theoretical derivation (Stokseth, 1969), the function S_z is strictly symmetrical in terms of the defocus path length error and not in terms of the defocus distance. However, the deviations from symmetry for ideal high-NA lenses are quite small within the defocus range of ± 5.0 μm, and for our purposes can be neglected.

Unfortunately, many assumptions of ideality go into the calculation of the two-dimensional OTFs. The errors introduced by these assumptions become significant for high-NA lenses and are further exaggerated when calculating three-dimensional OTFs. Alternatively, it is possible to determine the three-dimensional OTF experimentally by recording a set of images of a point source at different amounts of defocus. These images can be Fourier transformed in two dimensions to yield the $S_z(u, v)$ required by Eq. 3, or directly Fourier transformed in three dimensions.

MATERIALS AND METHODS

Microscope system

The microscope system used for these studies was built around a Zeiss inverted Axiomat microscope equipped with a liquid nitrogen-cooled (−120°C) 640 × 1024 pixel CCD (Photometrics, Ltd., Tucson, AZ). Microscope focus control and data collection are controlled by menu-driven software running on a VAX 8650 computer system. The cooled CCD is a nearly ideal imaging device for biological microscopy, combining high sensitivity, extreme linearity, a wide dynamic range, and geometric accuracy (Hiraoka et al., 1987). These properties are absolutely essential for accurate quantitation of fluorescent images. Digital resolution of the CCD data is 14 bits per pixel (16,384 grey levels); pixel size is 60 nm at the object plane with 63× objective lenses. Data collection of the bead images was done using on-chip summation of 2 × 2 pixels to give improved sensitivity with an effective pixel size of 0.12 μm and a total image size of 320 × 512.

OTF determination

Small polystyrene beads (90 nm in diameter) coated with a fluorescent dye (Pandex Laboratories, Inc., Mundelein, IL) having an emission spectrum of 470–530 nm (maximum at 490 nm) were used as point light sources. A 450–490–nm band-pass exciter filter, 510-nm dichroic mirror, and a 520–560–nm band-pass barrier filter were used. For examining the OTF of the oil immersion objective lens (Leitz 63 ×/NA = 1.4), the fluorescent beads were dried onto coverslips. The coverslip was reversed and placed on 2-μl of glycerol on a glass slide so that the beads were mounted in glycerol on the underside of the

coverslip; the coverslip was sealed with nail enamel to establish the physical stability of the specimen during data collection. Residual spherical aberration in the objective lens will seriously degrade the three-dimensional imaging capabilities of the microscope and lead to a very asymmetric PSF (Hiraoka et al., 1987). Immersion oils with a variety of refractive indices (η_D^{25} = 1.460 – 1.640 at an interval of 0.002 (R. P. Cargille Labs, Inc., Cedar Grove, NJ) where η_D^{25} refers to the refractive index at 25°C for the sodium D line, 589 nm) were used to alter the optical path length. To examine the effect of the mounting medium layer thickness on the optical behavior, we used four-well glass slides (Cel-Line, Inc., Newfield, NJ). The beads were dried onto the bottom of the wells; the wells were filled with glycerol and covered by a coverslip. The beads were attached also on the coverslip and used to measure the depth of the glycerol layer. The point images were obtained from the beads on the bottom of the wells. For the coverslip-free water-immersion objective lens (Zeiss 63×/NA = 1.2), the beads were dried onto a glass slide and imaged in buffer A without a coverslip (buffer A: 15 mM 1,4-piperazine-diethanesulfonic acid, pH 7.0, 80 mM KCl, 20 mM NaCl, 0.5 mM EGTA, 2 mM EDTA, 0.5 mM spermidine, 0.2 mM spermine, 0.1% 2-mercaptoethanol). Buffer A is routinely used during our investigations of chromosomes because it optimally preserves their structure (Belmont et al., 1989). Buffer A has no significant effects on the imaging properties of the microscope and behaves optically like water. Three-dimensional images of the single beads were recorded on the CCD as a set of 36 images from $z = -3.5$ to $+3.5$ μm, taken at 0.2-μm focal intervals. To improve the signal-to-noise ratio, which was especially important at large amount of defocus, the several beads on each image section were superimposed by a two-dimensional least-squares fitting procedure and subsequently averaged. The field of view was sufficiently small that point images were spatially invariant over the CCD field as shown by standard deviation statistical analysis, making each bead optically equivalent. The superimposed bead images from each section were radially averaged about a center of rotational symmetry as determined by least-squares fitting of the original and 180° rotated images. The radial two-dimensional OTF was calculated by Fourier-Bessel transformation of the radially-averaged bead image:

$$F(q) = 2\pi \int_0^\infty f(r) J_0(2\pi qr) r \, dr,$$

where $J_0(x)$ is a zero-order Bessel function. The three-dimensional OTF was calculated by direct three-dimensional Fourier transformation of the aligned and averaged stack of bead images and then cylindrically averaged in Fourier space.

Measurement of illumination intensity

Illumination intensity was estimated using a thin uniform layer of a fluorescent dye, rhodamine, sandwiched between a coverslip and a slide. 2 μl of glycerol containing rhodamine dye was put on a glass slide and covered with a coverslip (thickness No. 1.5 (0.17 mm), 22 × 22 mm); the excess glycerol was removed by pressing the coverslip until the thin-layer interference appeared so that the specimen thickness was estimated to be one-fourth of visual light wavelength, effectively behaving as a two-dimensional specimen. This sample was imaged on the CCD at 1-μm focal intervals, using the Leitz 63×/NA = 1.4 oil immersion objective lens and η_D^{25} = 1.515 immersion oil. A 546-nm band-pass exciter filter, a 580-nm dichroic mirror, and a 590-nm-long wavelength-pass barrier filter were used. The intensity along the optical center was calculated by averaging the intensity of the five most central pixels for each focal plane.

The variation in illumination dose with focus was also measured by integrating the total intensity emitted from a single bead at varying amounts of defocus. These measurements were repeated for a variety of circular apertures (0.05, 0.1, 0.16, 0.25, 0.4, 0.63, 1.0, 1.6, and 2.5 mm diameter) placed in the epiillumination field diaphragm position. Using a 63× objective lenses in our microscope system, these apertures illuminate a circular area with a diameter of 1.8, 3.6, 5.8, 9.0, 14, 23, 36, 58, and 90 μm, respectively, in the infocus object plane. To facilitate comparison with the dimensions of biological specimens, aperture sizes will hereafter refer to the diameter of the area illuminated in the object plane.

RESULTS

Optical properties of an epifluorescence microscope system were characterized using small (~emission wavelength/5) fluorescently-labeled beads as point light sources. The PSF was determined by recording point images on the CCD detector at different amounts of defocus above and below the object plane. For the measured data to correspond to the microscope's PSF, it is very important that the bead size be small compared to the diffraction limit. If this is not the case, the measured data will instead correspond to the convolution of the PSF with the bead shape. For beads larger than ~0.2 μm and at small values of defocus, the result will be dominated by the bead shape and not by the PSF. Unfortunately, the use of very small beads places stringent requirements on detector sensitivity. The exceptional sensitivity, photometric linearity, and geometric fidelity of the CCD was essential for obtaining accurate data with the very small beads. Two- and three-dimensional OTFs were calculated from averaged bead images by Fourier transformation as described in Methods. In this report, the following notation is used for OTFs: OTF(u, v, w) for a three-dimensional OTF, where (u, v, w) are reciprocal coordinates of (x, y, z); OTF(q, w) for the cylinderically-averaged OTF(u, v, w), where $q = (u^2 + v^2)^{1/2}$; OTF(q; z) for a radially-averaged, two-dimensional OTF for the z focal plane.

Partial confocal effect in epifluorescence microscopy

In epifluorescence microscopy, illumination is made through the objective lens, therefore changes in the excitation light are likely to occur as the focus is varied. If the effect were significant, this might affect the image-forming properties of the microscope. To examine this, we first measured the intensity in the center of the field of a uniform two-dimensional fluorescent object as a function of focal distance along the optical axis. As shown in Fig. 1, the smaller illumination field diameter gave the sharper intensity falloff. This effect was significant for high-NA objective lenses (NA = 1.2–1.4), but for a low-NA objective lens (NA = 0.5) the intensity was essentially invariant with focus up to ±10 μm. Note that this measure-

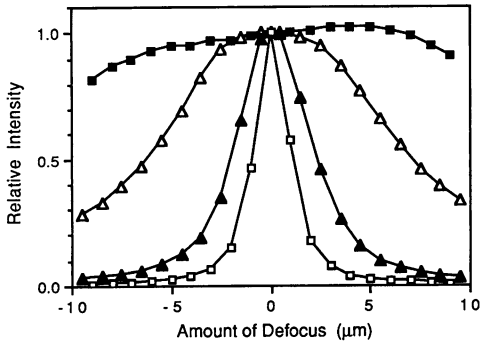

FIGURE 1 Illumination intensity as a function of defocus. A thin layer of fluorescent dye was imaged through the microscope with a Leitz 63×/NA = 1.4 oil objective lens. The intensity on the optical axis is plotted as a function of defocus. Symbols for the different diameters of illumination field are: 1.8 μm (□), 3.6 μm (▲), 14.4 μm (△), and 90 μm (■).

ment was made from plane images taken through a microscope instead of directly detecting the intensity at the object plane.

Another measurement, which provides information directly related to the OTF analysis, was performed by illuminating a single fluorescent bead and recording images while changing the microscope focus. The total intensity at each focal position was determined by integrating the density values in each image. The integrated intensity corresponds to the OTF value at $q = 0$ (OTF[0;z]). The resolution in the z direction can be evaluated by considering the falloff rate of OTF(0; z) as a function of defocus (z); the faster the falloff, the higher the resolution. Conventional imaging theory indicates that the integrated intensity should be independent of focus (hence no z-axis resolution).

Fig. 2 shows point images obtained with a coverslip-free water-immersion objective lens using different sizes of the illumination field. With a pinhole aperture (making a 1.8-μm-diameter illumination field), the PSF fell off more quickly as the amount of defocus increased compared with that for a wide-open diaphragm (producing a 90-μm-diameter illumination field).

The experimental data for integrated intensity plotted as a function of the amount of defocus for various sizes of illumination field is shown in Fig. 3. A pinhole aperture was centered on the optical axis and a single fluorescent bead was carefully positioned at the center of the aperture using the cross-hairs on the microscope. The upper panel of Fig. 4 *A* shows images of the single fluorescent bead at −2 μm defocus illuminated through different aperture sizes. It is clear that the defocused excitation is strongly dependent on illumination field size, decreasing with decreasing size. That this is not simply due to variations in the total illumination intensity is clear because the variation with aperture size does not occur at zero defocus (Fig. 4 *A*, *lower panel*). Fig. 4 *B* shows the integrated intensity at −2 μm defocus as a function of illumination

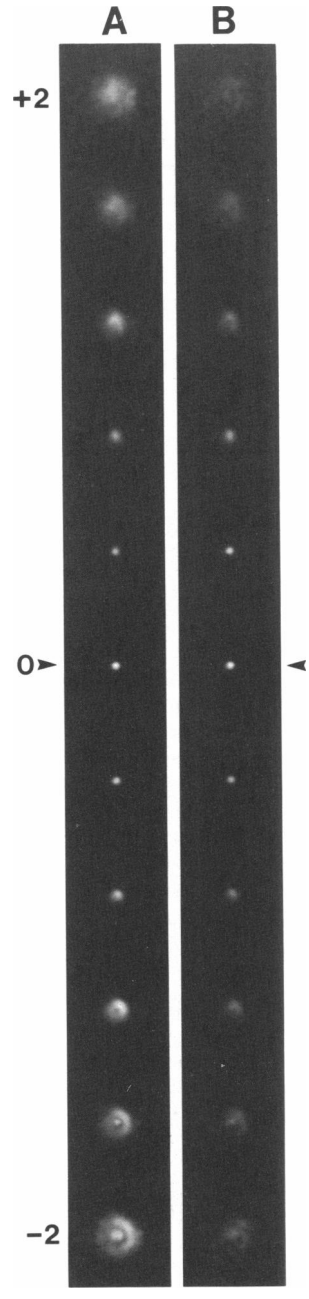

FIGURE 2 PSF for a water-immersion coverslip-free objective lens. The PSFs for the Zeiss 63×/NA = 1.2 coverslipless water immersion lens are shown for two different diameters of illumination field, 90 μm (*A*) and 1.8 μm (*B*). Numbers represent the defocus amount in micrometers; negative values of defocus correspond to the objective lens moving towards the specimen. The defocused images were scaled up by an arbitrary amount for display purposes.

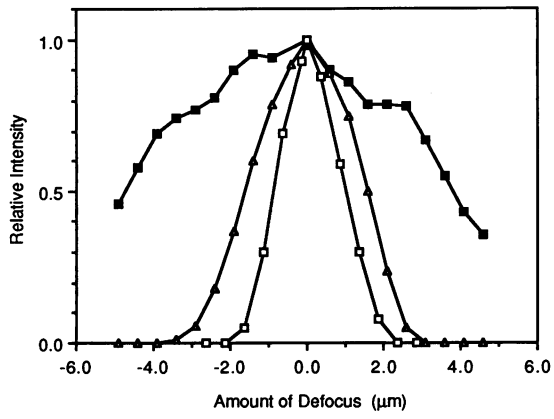

FIGURE 3 Integrated intensity of point images for a defocus series. A single fluorescent bead was illuminated at differing focal plane and the total intensity fo the spread point image was integrated. The integrated intensity was plotted as a function of defocus. Symbols for the diameters of illumination field: 1.8 μm (□), 14.4 μm (△), 90 μm (■).

field diameter. The smaller illumination field gave the sharper falloff as a function of defocus. These results indicate that in epifluorescence microscopy, using a smaller illumination aperture reduces the amount of out-of-focus image contamination and provides increased resolution in z direction.

Three-dimensional OTF of a microscope

Theoretical calculations of the OTF for a difraction-limited light microscope generally assume paraxial optical behavior with the illumination being independent of focal position. However, our results indicate that epifluorescence illumination actually causes a partial confocal effect, resulting in resolution along the z-axis. Conventional OTF calculations do not take this into consideration. As the degree of confocality depends upon the aperture choice, it is important to determine the OTF under the conditions actually used for imaging biological specimens.

Initially, we examined the microscope's PSF under standard conditions, i.e., the recommended coverslip thickness and immersion oil. All high-NA objective lenses tested (1.0–1.4) showed optical aberrations to various degrees, whereas low-NA lenses (0.4–0.7) showed little or no aberration. The two most significant aberrations observed were the lack of circular symmetry in the defocused images and the significant asymmetry of PSF above and below the focal plane. This latter distortion results from residual spherical aberration in the objective lens caused by errors in the optical path length within the microscope. It can be corrected by changing the refractive index of the immersion medium, by adjusting the correc-

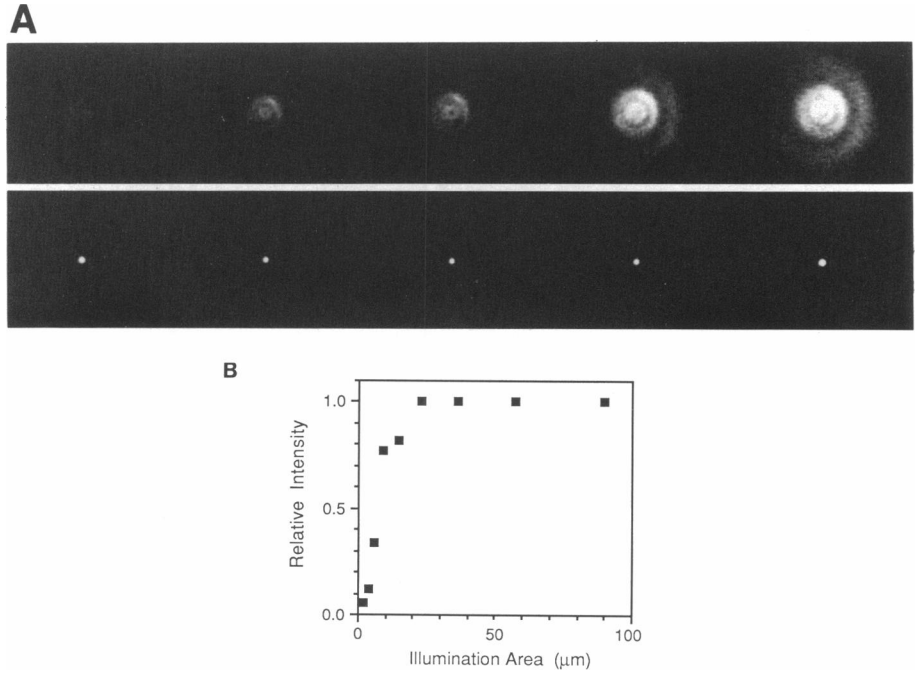

FIGURE 4 Point images recorded with varying illumination field diameters. (*A*) Defocus (−2 μm) and infocus bead images are shown with a grey scale of 0–1,000 and 0–5,000, in top and bottom, respectively. Exposure times are 20 s (defocus) and 2 s (infocus). Illumination field diameters are, from left to right, 1.8, 3.6, 5.8, 9.0 and 14.4 μm. These images were taken using the same single bead. (*B*) Integrated intensity is plotted as a function of the illumination field diameter.

tion collar on lenses so equipped, or directly altering the tube length to change the optical path length (Cagnet et al., 1962; Inoué, 1986).

To illustrate this point, Fig. 5 shows sections through the three-dimensional PSF recorded with immersion oils having refractive indices ranging from η_D^{25} = 1.510–1.530. The point images for the refractive indices η_D^{25} = 1.510, 1.518, and 1.530 are shown (Fig. 5 *B*) together with a profile of the center intensity as a function of defocus for each refractive index (Fig. 5 *A*). Using η_D^{25} = 1.510 oil, a series of strong rings were observed on one side (−) of the focal plane but not the other; this behavior is characteristic of an optical path length that is too short. Conversely, with η_D^{25} = 1.530 oil, the strong rings appeared on the other side (+) of the focal plane, as expected for a too long optical path. This behavior can be seen more clearly in *x-z* cross-section views (Fig. 5 *C*), where the PSFs show an approximately conical appearance very reminiscent of the

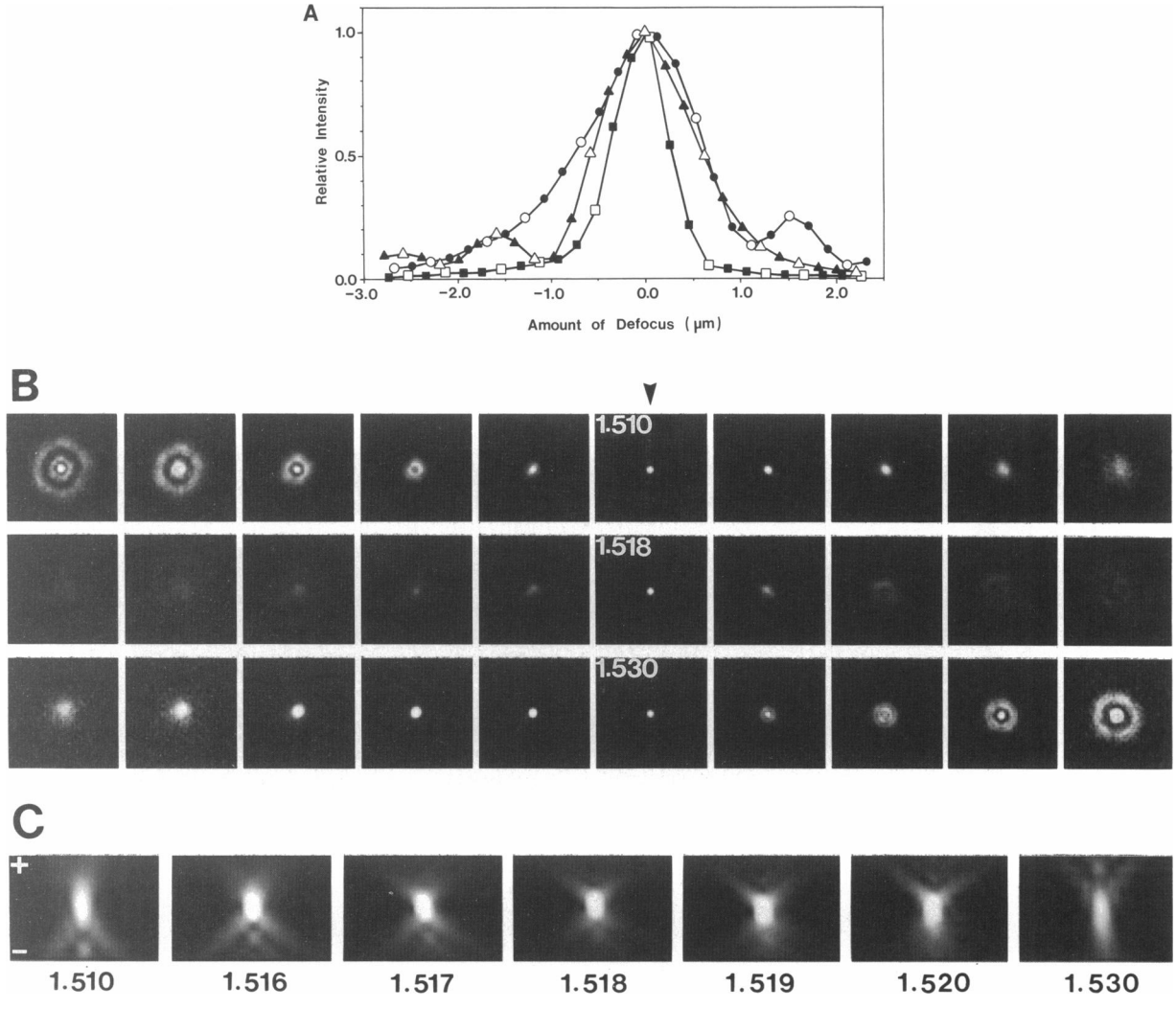

FIGURE 5 PSF data for differing immersion oil refractive indices. (*A*) The center intensity of each point image is plotted as a function of the amount of defocus. Negative values of defocus correspond to the objective lens moving towards the specimen. Symbols for the refractive indices of immersion oil: 1.510 (▲), 1.518 (■), and 1.530 (●). (*B*) Point images at a various defocus amount are shown for three refractive indices 1.510 (*top*), 1.518 (*middle*), and 1.530 (*bottom*). These images correspond to observations at defocus values denoted by the open symbols (△, □, ○) in *A*, in the same order from left to right. Arrowhead indicates the infocus position. Data for different refractive indices were normalized by comparing peak heights at 0 defocus; the 1.510 and 1.530 data were scaled to the 1.518 set. To simultaneously display the intense images taken near focus and the faint defocused images, it was necessary to multiply the images by an arbitrary scaling factor according to the amount of defocus; these scaling factors are 1 for infocus, 2 for ±0.6 μm defocus, 4 for ±1.2 μm and ±1.6 μm defocus, 15 for ±2.2 μm, and −2.6 μm defocus. (*C*) *x-z* cross-section views of the PSFs for differing refractive indices are shown. The numbers at the bottom are the refractive indices, and the +, − symbols indicate the direction of the defocus.

missing cone effects seen in electron microscopy (Agard and Stroud, 1981). This clearly shows how regions within the image contribute to the out-of-focus image contamination. The conical appearance was significantly asymmetrical about the focal plane at $\eta_D^{25} = 1.510$ and became symmetrical as the refractive index increased. The most symmetric pattern was obtained with $\eta_D^{25} = 1.518$. Further increases in refractive index generated asymmetry to the opposite side.

The resolution in the z direction was evaluated by considering the rate of the OTF falloff as a function of defocus as described above. Radially-averaged two-dimensional OTFs were calculated for each focal step and compared as a function of the refractive index. The OTF falloff at a spatial frequency of 0.16 μm^{-1} was plotted for $\eta_D^{25} = 1.510$, 1.518, and 1.530 immersion oils (Fig. 6). This spatial frequency was chosen because artifacts related to the finite size of the box surrounding each bead have their significant effects within the first node of the sinc function corresponding to that box size, whereas such artifacts are virtually eliminated at the node of the sinc function (0.16 μm^{-1}). The falloff of the OTF at a spatial frequency of 0 μm^{-1}, OTF(0; z) was also examined. In either case, the sharpest falloff in OTF on both sides of the focal plane was obtained with $\eta_D^{25} = 1.518$, the same refractive index that gave the most symmetrical PSF. Therefore, a simple and practical way to obtain the highest resolution in three dimensions is to select conditions that make the most symmetrical PSF.

In the above experiment, the fluorescent beads were attached directly to the underside of the coverslip to be consistent with the fact that objective lenses are designed to be optimally corrected for objects located immediately below the coverslip. In practice, during the observation of

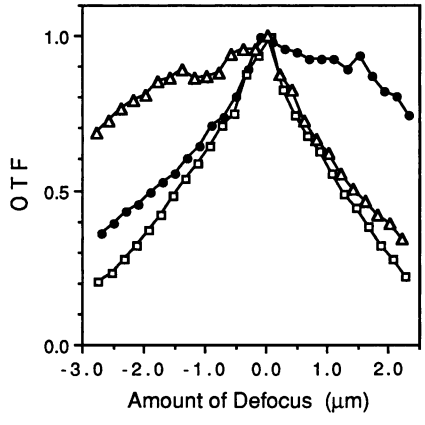

FIGURE 6 OTF falloff for differing immersion oil refractive indices. The value of the radially-averaged two-dimensional OTFs at a spatial frequency of 0.16 μm^{-1} are plotted as a function of defocus. Symbols for the refractive indices of immersion oil: 1.510 (△), 1.518 (□), and 1.530 (●).

biological specimens it is not always possible to place the specimen on a coverslip; instead specimens are often mounted using a mounting medium such as glycerol or buffer. This layer of mounting medium can also contribute to the total spherical aberration. For instance, fluorescent beads that were placed on a glass slide and mounted in a 32-μm layer of glycerol showed the asymmetry pattern characteristic of a short optical path length, when examined with an immersion oil of refractive index $\eta_D^{25} = 1.518$. This was due to the refractive index of glycerol ($\eta_D^{25} = 1.417$) being lower than that of glass; symmetry could be restored by using an $\eta_D^{25} = 1.528$ immersion oil.

For relatively thin specimens, the spherical aberration caused by the mounting medium itself can be minimized simply by removing excess mounting medium to place the specimen as close as possible to the coverslip. Unfortunately, the three-dimensional analysis of thick specimens poses a more difficult problem. Thus optimal conditions have to be determined for each type of specimen preparation based on attaining a symmetrical PSF. Ideally, high-NA objective lenses should be equipped with correction collars to allow rapid optimization of the optical path length for each three-dimensional object. The key point here is that real viewing conditions for biological specimens are often far from ideal, and if the optical path length is not taken into account, the resultant images can be seriously degraded.

Another way to avoid this problem is to use an objective lens that is designed to be used without a coverslip, thereby eliminating the potential discontinuity in index of refraction caused by the coverslip. For this reason we also determined the OTF of a Zeiss coverslip-free, water immersion objective lens 63×/NA = 1.2. The PSF images from fluorescent beads dried on a glass slide and imaged in buffer A without a coverslip were previously shown in Fig. 2. Without further corrections such as changing the index of refraction of the media, the PSF was nearly symmetrical about the focal plane.

Three-dimensional OTFs determined for the water-immersion objective lens, together with the theoretical OTF, are shown in the form of grey-level images of the cylindrically-averaged OTF(q, w) in Fig. 7. The OTFs shown in Fig. 7, *B* and *C*, were made from the PSFs in Fig. 2, *A* and *B*, respectively, for different aperture sizes. The values of OTF(0, w) and OTF(q, 0) are plotted as a function of spatial frequency in Fig. 8. The experimental OTFs are strikingly different from the theoretical one (Fig. 7 *A*), especially at low frequencies. In the theoretical OTF, no information is available at $q = 0$, due to the missing cone effect. In contrast, the experimentally determined OTFs do contain information at $q = 0$ (Fig. 7 *B*). However, the cutoff frequency at $w = 0$ is lower in the experimental OTF than in the ideal theoretical case, presumably because of residual optical aberrations. The

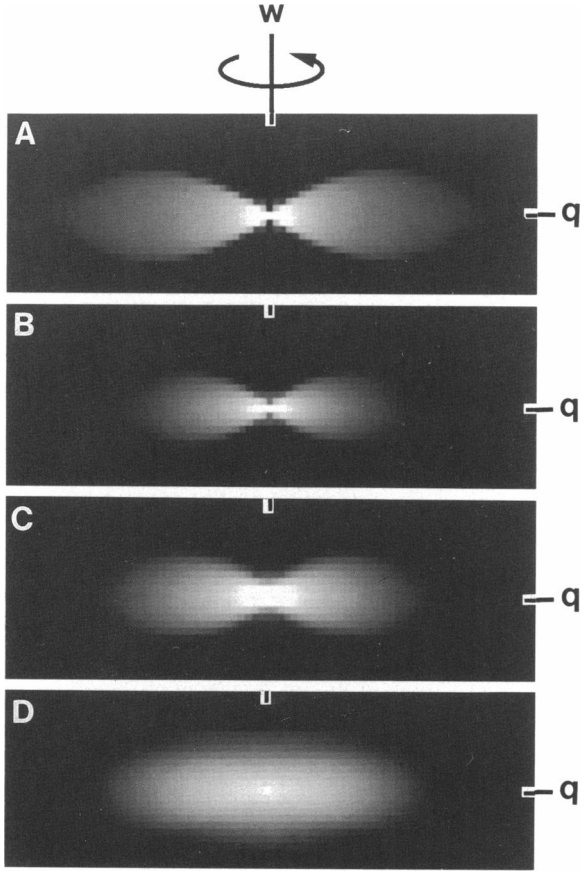

FIGURE 7 Cylindrically-averaged three-dimensional OTFs. (*A*) Theoretically-calculated OTF. Experimentally-determined three-dimensional OTFs for the Zeiss coverslip-free water-immersion objective lens (63×/NA = 1.2) for apertures producing 90 μm (*B*) and 1.8 μm (*C*) illumination fields at the specimen plane. (*D*) Frequency response of a deconvolved bead image taken using the aperture producing a 90-μm illumination field. Note the dramatic increase in *w*-axis resolution. All the images are displayed on a logarithmic scale to show intensities ranging over several orders of magnitude. To make a complete three-dimensional OTF, rotate the OTF about the *w*-axis as shown at the top of the figure.

strength of the OTF at low frequencies was shown to depend on the size of the aperture used, with the smaller aperture giving the stronger signal (Fig. 7 *C*). Use of the smaller aperture results in a slower falloff of OTF(0, *w*); that is, it provides more information in *z*. (Note that because OTF[*q*, *w*] is a one-dimensional Fourier transform of OTF[*q*; *z*], the slower falloff in OTF[*q*, *w*] corresponds to the faster falloff in OTF[*q*, *z*].) This unexpected increase in resolution along the focal direction (*z*) is explainable as a partial confocal behavior when using epiillumination with a high-NA objective lens as described above. Furthermore, when the three-dimensional bead data corresponding to Fig. 2 *A* was deconvolved by an iterative deconvolution method (Agard et al., 1989) using the corresponding OTF (Fig. 7 *B*), a significant amount of low-frequency information was recovered (Fig. 7 *D*).

DISCUSSION

For optimal high-resolution three-dimensional light microscopy, it is necessary to correct for the limitations inherent in the light microscope. Our approach for improving resolution and removing the out-of-focus information is to computationally deconvolve the observed microscopic image using the experimentally-determined OTF. For a complete discussion of deconvolution approaches see Agard et al. (1989).

We have demonstrated the direct measurement of the three-dimensional OTF for an epifluorescence microscope under a variety of light conditions. From this has come a better understanding of the three-dimensional imaging properties for the light microscope and awareness of how to optimize three-dimensional microscopy by minimizing spherical aberration. It should be emphasized that the experimentally-determined OTF is strkingly different from the theoretical one, especially at low spatial frequencies. In fact, the difference between the OTFs determined for the 1.4-NA Leitz oil immersion lens and the 1.2-NA Zeiss coverslipless water immersion lens was much smaller than that between the determined and theoretical OTFs. Thus, it may be practical to provide a reasonable estimate of the imaging properties of other high-resolution lenses by interpolation from those observed here.

The discrepancies between the observed and theoretical OTFs are a direct consequence of the partial confocal behavior observed in epiillumination with a high-NA objective lens. This partial confocal behavior, in turn, is a direct consequence of the decreased excitation intensity that occurs with increasing defocus. The use of smaller illumination apertures improves not only contrast, as is well known, but also the *z* resolution in epifluorescence microscopy.

Eq. 1 can now be extended to include the effect of the distribution of the excitation light, $g(x, y, z)$ on the PSF:

$$i(x, y, z) = o(x, y, z) * [s(x, y, z) \cdot g(x, y, z)], \quad (4)$$

where the * represents the short-hand form of the convolution integral. For transmitted illumination, $g(x, y, z)$ is constant and we again obtain Eq. 1. For the situation described here, $g(x, y, z)$ should be related to the convolution of the PSF with the aperture function $a(x, y, z)$:

$$g(x, y, z) = s(x, y, z) * a(x, y, z). \quad (5)$$

For truly confocal illumination, $a(x, y, z)$ is a delta

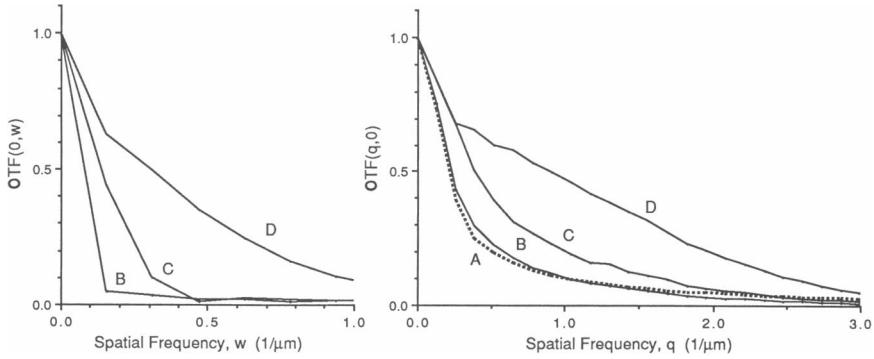

FIGURE 8 Falloff of the experimental three-dimensional OTF. The values of OTF(q, w) at $q = 0$ (*left*) and $w = 0$ (*right*) are plotted. Labels *A–D* refer to the OTFs in Fig. 7. In left panel, the plot for the theoretical OTF (Fig. 7 *A*) is not shown because the function OTF(0, w) is nonzero only at $w = 0$

function and $g(x, y, z)$ is equivalent to the PSF. Therefore, as previously reported (Wilson and Sheppard, 1984):

$$i(x, y, z) = o(x, y, z) * s(x, y, z)^2. \quad (6)$$

Thus, epiillumination shows an intermediate behavior between transmitted illumination and confocal illumination. It should be noted, however, that epifluorescence microscopes have no detector pinhole unlike confocal microscopes and do not reject the out-of-focus information.

The measured three-dimensional OTF has been used in our laboratories for the routine three-dimensional analysis of a vast range of specimens including yeast, *Drosphila melanogaster* embryos, *Drosophila* Kc tissue culture cells, and several lines of mammalian tissue culture cells. Although there may be instances where the OTF must be determined under the identical conditions for the individual observation, in general we use the determinations made for these two lenses as models for other lenses. The methods described for the characterization of optical properties of epifluorescence microscope system are quite general, and could be applied to other light microscope systems. Using this approach, it should also be possible to significantly improve images derived from confocal microscopy.

This work was supported by grants from National Institute of Health to J. W. Sedat (GM-25101) and D. A. Agard (GM-31627) and by the Howard Hughes Medical Institute (J. W. Sedat and D. A. Agard). D. A. Agard is also a National Science Foundation Presidential Young Investigator. Y. Hiraoka was supported by Damon Runyon-Walter Winchell Cancer Research Fund Fellowship DRG903.

Received for publication 5 June 1989 and in final form 18 October 1989.

REFERENCES

Agard, D. A. 1984. Optical sectioning microscopy: cellular architecture in three dimensions. *Annu. Rev. Biophys. Bioeng.* 13:191–219.

Agard, D. A., and R. M. Stroud. 1981. Linking regions between helices in bacteriophodopsin revealed. *Biophys. J.* 37:589–602.

Agard, D. A., Y. Hiraoka, P. Shaw, and J. W. Sedat. 1989. Fluorescence microscopy in three dimensions. *Methods Cell Biol.* 30:353–377.

Belmont, A. S., M. B. Braunfeld, J. W. Sedat, and D. A. Agard. 1989. Large-scale structural domains within mitotic and interphase chromosomes in vivo and in vitro. *Chromosoma (Berl.).* 98:129–143.

Bracewell, R. N. 1965. The Fourier Transform and Its Applications. McGraw-Hill Book Co., New York.

Cagnet, M., M. Francon, and J. C. Thrierr. 1962. Atlas of Optical Phenomena. Springer-Verlag/Prentice-Hall, Englewood Cliffs, NJ.

Castleman, K. R. 1979. Digital Image Processing. Prentice-Hall, Englewood Cliffs, NJ.

Erhardt, A., G. Zinser, D. Komitowski, and J. Bille. 1985. Reconstructing 3-D light-microscopic images by digital image processing. *Appl. Optics.* 24:194.

Hiraoka, Y., J. W. Sedat, and D. A. Agard. 1987. The use of charge-coupled device for quantitative optical microscopy of biological structures. *Science (Wash. DC).* 238:36–41.

Hopkins, H. H. 1955. The frequency responce of a defocused optical system. *Proc. R. Soc. (Lond.)* A231:91–103.

Inoué, S. 1986. Video Microscopy. Plenum Publishing Corp., New York.

Sheppard, C. J. R. 1987. Depth of field in optical microscopy. *J. Microsc.* 149:73–75.

Stokseth, P. A. 1969. Properties of a defocus optical system. *J. Opt. Soc. Am.* 59:1314.

Waggoner, A., R. DeBiasio, P. Conrad, G. R. Bright, L. Ernst, K. Ryan, M. Nederlof, and D. Taylor. 1989. Multiple spectral parameter imaging. *Methods Cell Biol.* 30:449–478.

Wilson, T., and C. J. R. Sheppard. 1984. Theory and Practice of Scanning Optical Microscopy. Academic Press, Inc., London.